A Receding Interface Model for the Drying of Slurry Droplets

A receding interface model of the drying of single drops of slurries of sodium sulfate decahydrate has been developed to describe the drying characteristics of this material and to estimate the drying rates of particulate slurries. The simultaneous heat and mass transfer rate equations have been solved numerically, and the results obtained have been compared with those obtained experimentally by drying single drops suspended on the tip of a glass filament.

Single drops of slurries, 1.0 to 1.5 $\times$ 10^{-3} m dia., were suspended on the tip of a flexible glass cantilever inserted in a vertical wind tunnel. A 50μm dia. nickel wire passed through the center of the glass beam and the outer surface was coated with a thin film of copper, thereby forming a thermocouple that measured the temperature of the core of the drop; the deflection of the beam gave the loss in weight during drying. In this way the instantaneous drying rate and drop temeprature were determined and compared with those predicted by the receding interface model. In all cases the agreement between the predictions of the model and experimental results was good.

H. W. Cheong, G. V. Jeffreys, C. J. Mumford
Department of Chemical Engineering
University of Aston
Birmingham, England

SCOPE

One of the prerequisites for the optimum design of processes involving evaporation of a spray is an understanding of the controlling mechanisms in the heat and mass transfer processes during drying. Although a great deal of fundamental research had been carried out on the evaporation of pure liquid drops (Whytlaw-Gray and Patterson, 1932; Langstroth et al. 1950; Ranz and Marshall, 1952; Pasternak and Gauvin, 1960), experimental data on the drying of drops containing solids is limited. This can be attributed in part to the complexities in analyzing the heat and mass transfer processes after a solid crust has formed. Heat is transferred by convection from the drying medium to the outer surface of the crust and then by conduction through the solid portion of the crust to the interior. Evaporation occurs and moisture diffuses through the pores in the crust into the surroundings. As the particle dries, the crust increases in thickness, resulting in an increase in the resistance to heat and mass transfer. This invariably decreases the core temperature, initially causing a reduction in the partial pressure driving force. However when the temperature of the core of the drop is considerably below that of the drying medium, the core temperature afterwards increases and the drying rate consequently increases. The transfer process is therefore highly complex and difficult to model mathematically.

The present study was initiated to further the understanding of the mechanisms involved in the drying of drops containing solids, and more specifically to formulate a mathematical model to predict the drying rate under conditions that might be encountered in spray-drying equipment.

CONCLUSIONS AND SIGNIFICANCE

The filament thermocouple developed for this investigation provided valuable insight into the drying process not normally obtainable from a simple mass balance.

The drying of suspended drops 1 to 1.5 × 10^{-3} m in dia. of aqueous sodium sulfate decahydrate solutions was characterized by two distinct drying periods, an initial constant period and a falling rate period as soon as a crust was formed. The receding interface model developed for the drying of slurry drops was found to be applicable to drops of sodium sulfate decahydrate slurries with an initial concentration of 40 wt. %, for which drying proceeds entirely in the falling rate period. However the drying of this material was demonstrated to be complicated by the enantiomorphic changes taking place at 33°C. When the heats of solution of the different hydrates and the heats of transition of the crystal forms were included in the model, the agreement between the predicted drying behavior of this complex material and experimental drying behavior over the temperature range 20 to 78°C was good.

The model is generally applicable to the drying of slurries, particularly those somewhat simpler in nature than sodium sulfate decahydrate, and has significance in the drying of drops of slurries in spray-drying equipment.

Mathematical Model for a Slurry Droplet

When a droplet containing dissolved or suspended solids is dried the vapor pressure at the drop surface is less than that of a drop of the solvent, with the result that there will be a reduction in the mass transfer rate. The surface temperature of the evaporating droplet will consequently increase above the thermodynamic wet-bulb temperature and the drying characteristics will be related to the formation of a solid phase at the surface of the droplet because an additional resistance to moisture transfer into the surrounding media has been introduced.

In the case of droplets containing dissolved solids, experimentation has shown that evaporation commences at a constant rate (Ranz and Marshall, 1952; Trommelen and Crosby, 1970; Charlesworth and Marshall, 1960) termed the initial drying period. When the droplet moisture content falls below a critical value a solid crust commences forming from a preferential site, usually the point of maximum mass transfer, and spreads around the droplet. As the crust thickens, the crust resistance becomes predominant and the evaporation rate decreases. This is classified as the falling-rate drying period. For drops containing suspended solids, vapor pressure lowering effects are generally negligible. Evaporation may commence with an initial constant period, but if it exists at all this will be very short, depending on the solids content. Once a solid crust is formed, the falling rate period follows.

The drying rate after crust formation is generally controlled by the resistance of the crust to vapor diffusion. Heat is transferred through the crust into the wet core where evaporation occurs at the interface between the core and the crust. The vapor then diffuses through the pores of the crust into the drying medium. Capillary effects are negligible and self-balancing; liquid sucked into one capillary must drain from another. On this basis consider a slurry droplet after a crust has been formed as depicted in Figure 1. Let the outer radius of the crust be $r = R$ and the evaporation interface be $r = z$. The following assumptions are made:

1. Evaporation only occurs at the evaporation interface, which is the interface between the wet core and dry crust.
2. The evaporation interface, $r = z$, recedes into the wet core as evaporation proceeds.
3. Once formed, the crust does not shrink or inflate, i.e., R remains constant. It is also assumed that no fracture occurs.
4. The core temperature, T_c, is uniform throughout the core.
5. Heat is transferred from the drying air to the crust solely by convection.
6. Heat is transferred through the crust by conduction.
7. The moisture is transferred from the evaporation interface by vapor diffusion through the pores, represented by an effective diffusivity D_{eff}.
8. The wet core density of the slurry remains constant during the evaporation process; i.e., as water evaporates at the interface

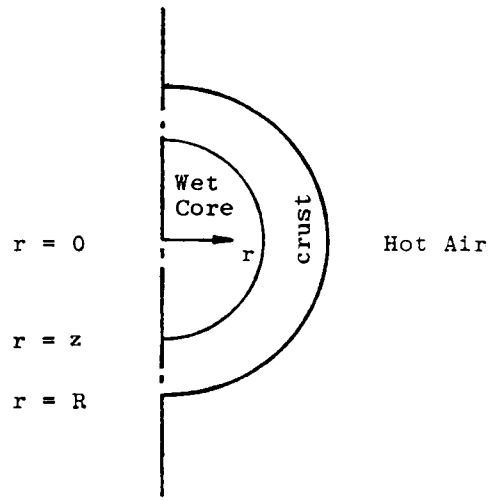

Figure 1. Spherical slurry droplet after crust formation.

it precipitates an equivalent amount of solid as crust, between the surface of the particle and the wet core. The core continues to be a slurry of density $\simeq 1.22$ kg/m^3.

9. The energy and water vapor storage within the crust are assumed to be negligible because the crusts produced are thin, i.e., of the order of 0.25×10^{-3} m (see Figure 13).

Then a heat balance over the evaporation interface at $r = z$ can be expressed as:

Rate of heat supplied through crust = Rate of heat loss by evaporation + Rate of sensible heat supply into core

or,

$$4\pi z^2 k_{tc} \left.\frac{\delta T}{\delta r}\right|_{r=z} = -4\pi z^2 \rho_{co} x(\lambda - C_c)\left(\frac{dz}{d\theta}\right) + \frac{4}{3}\pi z^3 C_{pc}\rho_{co}\left(\frac{dT_c}{d\theta}\right) \quad (1)$$

which reduces to

$$-\frac{dz}{d\theta} = \left[\frac{k_{tc}}{\rho_{co} x(\lambda - C_c)}\right]\left.\frac{\partial T}{\partial r}\right|_{r=z} - \left[\frac{C_{pc} z}{3x(\lambda - C_c)}\right]\frac{dT_c}{d\theta} \quad (2)$$

The final assumption (9) implies a linear temperature gradient within the crust. Then the rate of heat transfer can be expressed as

$$4\pi r^2 k_{tc}\frac{\partial T}{\partial r} = \text{constant} \quad (3)$$

Integrating Eq. 3 between the limits $r = R$ and $r = z$, gives

$$Q_r = 4\pi k_{tc}(T_R - T_z)\left(\frac{Rz}{R - z}\right) \quad (4)$$

At $r = R$,

$$Q_R = 4\pi k_{tc} R^2 \left.\frac{\partial T}{\partial r}\right|_R \quad (5)$$

and at $r = z$,

$$Q_z = 4\pi k_{tc} z^2 \left.\frac{\partial T}{\partial r}\right|_{r=z} \quad (6)$$

but, $Q_r = Q_R = Q_z$, so that

$$\left.\frac{\partial T}{\partial r}\right|_R = \frac{z(T_R - T_z)}{R(R - z)} \quad (7)$$

and

$$\left.\frac{\partial T}{\partial r}\right|_{r=z} = \frac{R^2}{z^2}\left.\frac{\partial T}{\partial r}\right|_R \quad (8)$$

but $T_z = T_c$ at the surface of the wet core so that Eq. 7 becomes

$$\left.\frac{\partial T}{\partial r}\right|_R = \frac{z(T_R - T_c)}{R(R - z)} \quad (9)$$

Also at $r = R$,

$$4\pi R^2 k_{tc}\left.\frac{\partial T}{\partial r}\right|_R = 4\pi R^2 h_g(T_g - T_R) \quad (10)$$

where h_g = gas film heat transfer coefficient.

Substituting Eq. 9 into Eq. 10 gives

$$(T_R - T_c) = \frac{R(R - z)h_g}{k_{tc} z}(T_g - T_R) \quad (11)$$

Let

$$a_0 = \frac{R(R - z)h_g}{k_{tc} z}$$

Rearranging gives

$$(T_R - T_c) = \left(\frac{a_0}{1 + a_0}\right)(T_g - T_c) \quad (12)$$

Substituting Eq. 12 into Eq. 9 and the resulting equation into Eq. 8 gives

$$\left.\frac{\partial T}{\partial r}\right|_z = \left(\frac{a_0}{1 + a_0}\right)\left[\frac{R}{z(R - z)}\right](T_g - T_c) \quad (13)$$

Substituting Eq. 13 and the value of a_0 into the heat balance, Eq. 2, gives

$$-\frac{dz}{d\theta} = \left[\frac{R^2 h_g k_{tc}}{\rho_{co} x(\lambda - C_c)}\right]\left[\frac{1}{(k_{tc} - Rh_g)z^2 + R^2 h_g z}\right] \cdot (T_g - T_c) - \left[\frac{C_{pc} z}{3x(\lambda - C_c)}\right]\frac{dT_c}{d\theta} \quad (14)$$

Let

$$a_1 = \frac{R^2 h_g k_{tc}}{\rho_{co} x(\lambda - C_c)} \qquad a_2 = k_{tc} - Rh_g$$

$$a_3 = R^2 h_g \qquad a_4 = \frac{C_{pc}}{3x(\lambda - C_c)}$$

Then Eq. 14 becomes

$$-\frac{dz}{d\theta} = \left(\frac{a_1}{a_2 z^2 + a_3 z}\right)(T_g - T_c) - a_4 z\frac{dT_c}{d\theta} \quad (15)$$

Mass transfer at evaporation interface

A mass balance over the evaporation interface for low rates of mass transfer pertaining to the conditions in the drying of par-

ticulate slurries can be expressed by

$$-4\pi z^2 \rho_{co} x \cdot \frac{dz}{d\theta} = -4\pi z^2 D_{\text{eff}} \left(\frac{M_w}{R_c T_c}\right) \cdot \left.\frac{\partial p}{\partial r}\right|_{r=z} \tag{16}$$

This reduces to

$$\frac{dz}{d\theta} = \left(\frac{D_{\text{eff}}}{\rho_{co} x}\right)\left(\frac{M_w}{R_c T_c}\right) \left.\frac{\partial p}{\partial r}\right|_{r=z} \tag{17}$$

As in the case of heat transfer, a linear concentration gradient can be assumed for the thin crusts. Hence, the rate of mass transfer can be expressed as

$$J_r = -4\pi r^2 D_{\text{eff}} \left(\frac{\partial p}{\partial r}\right) = \text{constant} \tag{18}$$

where D_{eff} is evaluated at the mean crust temperature.

A similar analysis to that for heat transfer yields,

$$\frac{dz}{d\theta} = \left(\frac{b_1}{b_2 z^2 + b_3 z}\right) \frac{(p_g - p_c)}{T_c} \tag{19}$$

Where b_0, b_1, b_2, b_3, etc. are functions as defined in the Notation. Equations 19 and 15 have to be solved simultaneously since they are coupled heat and mass transfer equations. Thus

$$\frac{dT_c}{d\theta} = \left(\frac{a_1/a_4}{a_2 z^2 + a_3 z}\right) \frac{(T_g - T_c)}{z} + \left(\frac{b_1/a_4}{b_2 z^2 + b_3 z}\right) \frac{(p_g - p_c)}{T_c z} \tag{20}$$

Also, from Eq. 16, the rate of mass transfer can be expressed as

$$-\frac{dW}{d\theta} = -4\pi z^2 \rho_{co} x \frac{dz}{d\theta} \tag{21}$$

Substituting for $dz/d\theta$ from Eq. 19 gives

$$-\frac{dW}{d\theta} = -4\pi z^2 \rho_{co} x \left(\frac{b_1}{b_2 z^2 + b_3 z}\right) \frac{(p_g - p_c)}{T_c} \tag{22}$$

Equations 19, 20, and 22 can be solved simultaneously by the Runge-Kutta fourth-order method to give the crust thickness, core temperature, and weight of the drop as a function of time, using the boundary conditions pertaining to the different experiments, i.e., air temperature, drop size, and solids content, with air velocities of 0.5 to 3 ms^{-1}. Solution requires an expression for the vapor pressure, p_c, at the evaporation interface, which is a function only of the core temperature: $p_c = f(T_c)$. An appropriation computer program (Cheong, 1983) was developed to solve the differential equations above using a microcomputer.

Experimental

The experimental apparatus comprised a wind tunnel that supplied drying air to the working section in which the drops were suspended. The drying characteristics of single droplets have conventionally been investigated by suspending them in humidity-controlled wind tunnels. In a horizontal wind tunnel, the suspended drop tends to be displaced slightly in the direction of the flow and the suspension device inevitably disturbs the flow pattern around the drop to some extent. In addition, free convection currents caused by differences in densities, which would normally flow vertically upward, would be dragged toward the wake of the drop. Conversely with upward flowing air in a vertical tunnel the suspension device resides in the wake of the drop, where it is least likely to disturb the flow. Convection currents also tend to move symmetrically around the drop with the flow, simulating more closely a drop in free flight. Consequently, a vertical wind tunnel with upward-flowing air was adopted for the present investigation.

Nozzles, capillaries, and glass filaments have been used previously for drop suspension. The nozzles used by Audu and Jeffreys (1975), had the disadvantage of having a similar diameter to the drop itself, resulting in a significant disturbance to the flow pattern of air around the drop. Heat conduction through the nozzle was also substantial because of the large surface area in contact with the drop. Conversely, glass filaments can be fabricated to very small diameters (0.17 mm), and therefore much smaller and more spherical drops can be studied. In the present study the suspension device incorporated a fine glass filament, of 0.176 to 0.2 mm dia. and 150 mm long, as shown in Figure 2. This suspension technique was previously used for the drying of liquid droplets by Frössling (1938), Trommelen and Crosby

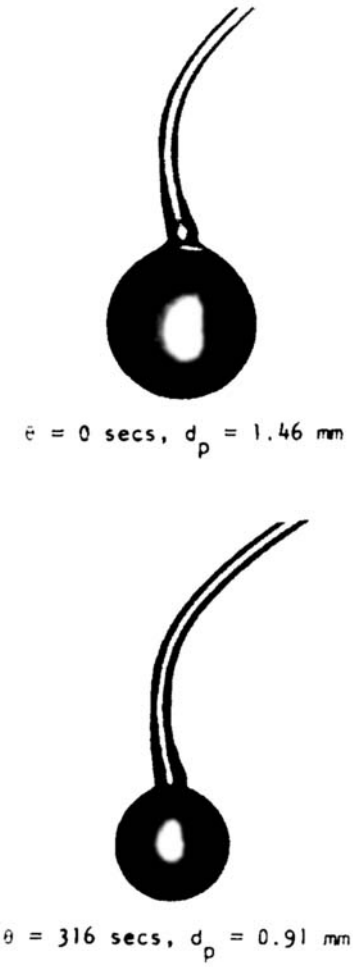

Figure 2. Method of drop suspension.

(1970), and Charlesworth and Marshall (1960) at temperatures ranging from 18° to 400°C. However, for this study a thermocouple was developed for the simultaneous measurement of evaporation rate and drop temperature during drying. A fine, 99% pure nickel wire (50 μm dia.) was inserted through a hollow glass filament (0.18 to 0.2 mm O.D. with a bore of 0.07 to 0.10 mm), and a thin film of copper was deposited onto the outside surface of the filament by applying a vacuum coating technique (Cheong, 1983). A junction was created at the tip of the filament where about 0.5 mm of nickel wire was exposed. The surface area of the drop in contact with the suspension filament was extremely small, less than 0.8%, and therefore heat conduction was minimal. The thin film thermocouple was a novel drop temperature-measuring device incorporating provision for simultaneous drop weight measurement, which in previous studies has been measured separately on supposedly identical drops. Nickel wire and copper film were chosen as the conducting elements because of their large thermal electromotive power change per degree change in temperature. The difference and hence sensitivity is therefore comparable to the more commonly used thermocouples. Although both nickel and copper films adhere readily to glass, the latter is more easily evaporated, having a melting point of 1,200°C at a pressure of 10^{-2} torr (1.33 Pa).

The surface area of the thermojunction of the thin film thermocouple was comparable to that of a conventional argon-welded junction, but being a single length 0.5 mm long, it was totally immersed and extended into the core of the particles. It therefore measured the core temperature throughout the majority of the drying period. The thermocouple had the further advantage of enabling accurate measurements to be made of temperature profiles in the crust of drops containing solids by using different lengths of exposed wire at the tip of the thermocouple.

The wind tunnel was designed to supply hot dry air at a constant humidity and temperature to the working section; a diagram of the tunnel is given in Figure 3. Compressed air, from the mains supply at 6.53 bar, was piped into a reservoir to dampen any fluctuations. The pressure was then reduced to 1.43 bar and the air dried by passage through a packed column of silica gel and aluminate-silicate molecular sieve in the horizontal industrial glass pipe section.

The inlet and outlet moisture contents of the air were measured during commissioning using a wet and dry bulb hygrometer. At ambient temperature, the outlet air was found to have a humidity of 0.1×10^{-3} kg/kg. This value did not deviate by more than 1.0%, provided that at least 25 mm of the molecular sieve packing remained unsaturated, as indicated by the absence of color change. Therefore, experiments were always conducted with at least this minimum amount of unsaturated desiccant.

The air flow rate was controlled by a needle valve and measured by a rotameter. The air was heated by two 1.0 kW electric heaters fitted inside an 0.08 m O.D. copper tube. The working section was fabricated from standard 0.028 m O.D. copper tube with two windows located midway up the vertical section, and the exit pipework was designed to recirculate the hot air over the air dryer for regeneration of the desiccants *in situ*.

Drop suspension

Pure water drops were suspended at the free end of a fine glass filament, (0.176 to 0.2 mm dia., 150 mm long) and the fixed end was held in a stainless steel clamp. The angular deflection was measured to estimate the weight of the drop and mea-

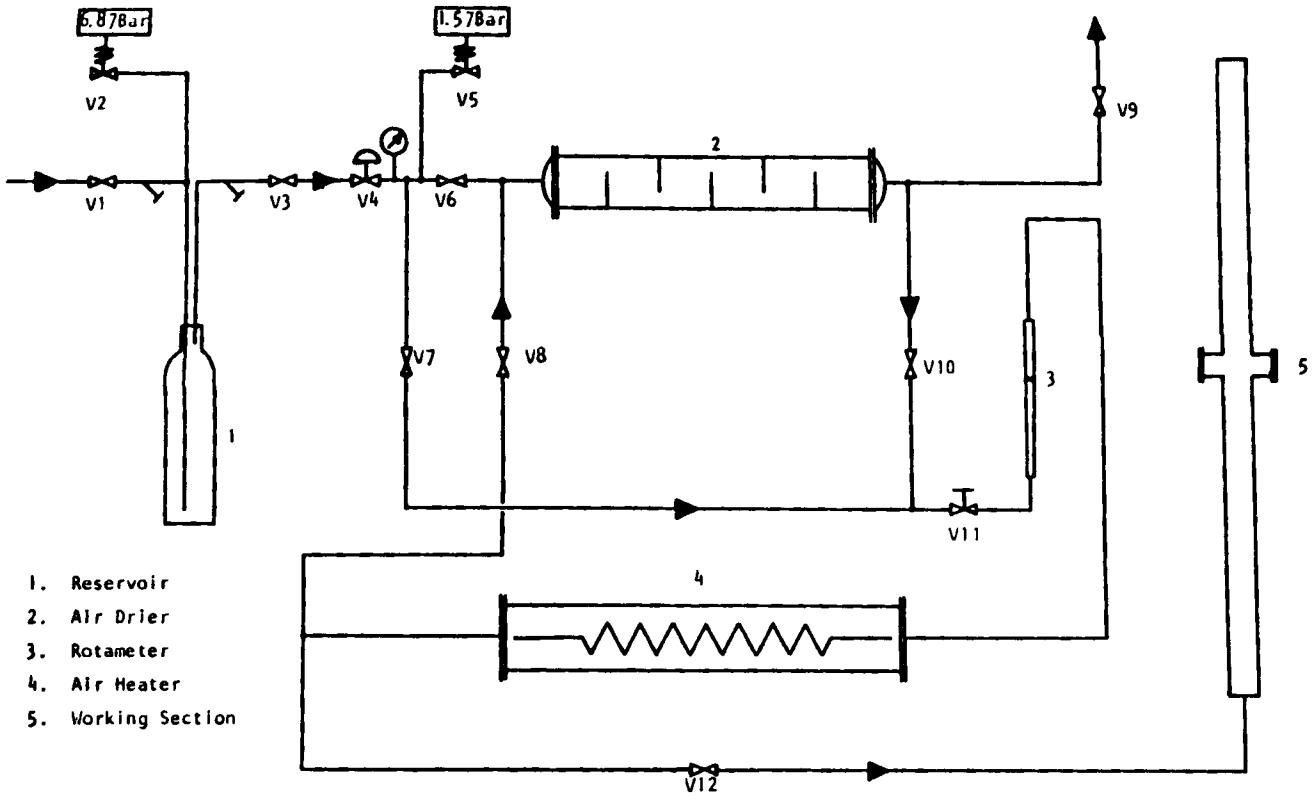

Figure 3. Schematic diagram of wind tunnel.

surements were always made at a distance of 25 mm from the free end of the filament to give the largest deflection-to-weight ratio.

Slurry drops were suspended from the thin film thermocouple, which was fabricated from a 250 mm long hollow glass filament as described above. The thin film thermocouple holder served as a cold junction reference for voltage measurements. It consisted of an ice box with a stainless steel needle tube fitted through it to form a cold junction pocket.

The weight of an evaporating drop was measured by the deflection of the glass filament, which was calibrated by attaching different lengths of cotton threads of known standard weights to the tip of the beam. A trace of petroleum jelly was smeared onto the tip of the filament to facilitate attachment of the cotton thread. A typical calibration curve of drop weight vs. deflection is shown in Figure 4. The measured deflections recorded during an experiment were always corrected for the drag force of the upward flowing air.

The total drag force, F_t, on the drop and the section of the filament inside the tunnel can be expressed as

$$F_t = F_d + F_f \tag{23}$$

where F_d = drag force on the spherical drop, and F_f = drag force on the filament.

For the drop,

$$F_d = C_d A_p \rho v^2/2 \tag{24}$$

and for the filament,

$$F_f = C_f A_f \rho v^2/2 \tag{25}$$

where C_d, C_f = drag coefficients for a sphere and cylinder, respectively, and A_p, A_f = projected areas for a sphere and cylinder, respectively.

For a typical experimental condition,

$v = 0.316\ \text{ms}^{-1}$ $d_p = 1.069 \times 10^{-3}$ m $d_f = 1.764 \times 10^{-4}$ m

$\mu = 1.8 \times 10^{-5}\ \text{kg} \cdot \text{ms}^{-1}$ $\rho = 1.205\ \text{kg} \cdot \text{m}^{-3}$

Length of filament inside tunnel = 12×10^{-3} m.

Hence, for the filament,

$Re_f = 0.316\,(1.764 \times 10^{-4})(1.205)/1.8 \times 10^{-5} = 3.73.$

The drag coefficient for a horizontal cylinder at a Reynolds number of 3.73 is 5 (Perry and Chilton, 1973). Therefore,

$F_f = 5\,(1.764 \times 10^{-4})(1.205)(0.316)^2/2 = 6.9 \times 10^{-7}$ N.

Similarly for the drop,

$Re = 0.316\,(1.069 \times 10^{-3})(1.205)/1.8 \times 10^{-5} = 22.6.$

The drag coefficient for a sphere at a Reynolds number of 22.6 is 4 (Perry and Chilton, 1973). Therefore,

$F_d = 3(\pi/4)(1.069 \times 10^{-3})^2(1.205)(0.316)^2/2 = 1.6 \times 10^{-7}$ N.

The total drag force caused by the upward flowing air is,

$F_t = (6.9 + 1.6) \times 10^{-7}\ \text{N} = 8.5 \times 10^{-7}.$

The actual weight of a suspended drop was therefore the measured weight (from the deflection) plus F_t/g.

The thicknesses of the crusts formed during drying of drops of slurry under different conditions were determined from Stereoscan microscope photographs. Porosities were determined from these photographs together with pressure drop measurements using a separate apparatus (Audu and Jeffreys, 1975).

Drop temperature

Drop temperatures were measured with the thin film glass filament thermocouple. The voltage output was measured with a Comark D.C. Microvoltometer and recorded on a chart recorder.

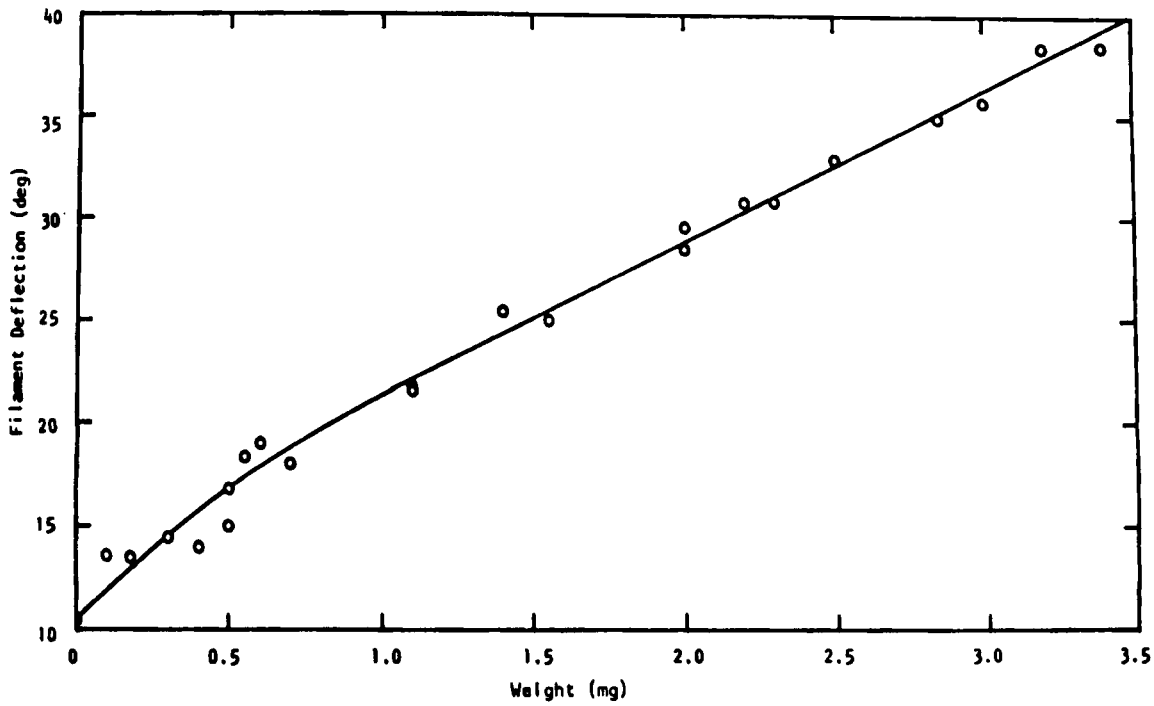

Figure 4. Glass filament calibration curve.

Dry air at velocity of 2.0 ms^{-1} in the working section of the wind tunnel was used as the uniform temperature source for calibration and the thin film thermocouple was calibrated against a standard Ni-Cr/Ni-Al thermocouple over a temperature range of 8.75 to 110.25°C. For the purposes of calibration, a glass helical coil was immersed in an ice bath and located between the air heater and the working section. Air was passed through the coil and was cooled to a temperature of 8.75°C by the addition of sodium chloride to the ice in the bath. For calibration at higher temperatures the air was heated by the air heater by addition of warm water to the bath surrounding the coil. Calibration curves for the thin film thermocouple could be accurately approximated by two linear sections and therefore linear regression analysis was applied. The resulting variation between voltage output and temperature was found to be,

$$T_s = 43.27\ V + 3.02 \text{ for } V \leq 1.1\ mV \tag{26}$$

and

$$T_s = 37.95\ V + 9.90 \text{ for } 1.1\ mV < V < 2.65\ mV \tag{27}$$

Results

Results for the evaporation of water drops are reported elsewhere (Cheong, 1983). At ambient temperature the data were correlated by the well-established equation:

$$Nu = 2 + \phi Re^{0.5} Pr^{0.33} \tag{28}$$

with $\phi = 0.66$, with a correlation coefficient of 0.98. This value compared well with values of 0.69 (Rowe et al., 1965), 0.625 (Miura et al., 1971), and 0.60 (Ranz and Marshall, 1952), and confirmed the reliability of the wind tunnel and drop suspension technique. At higher air temperatures in the range 19 to 79°C the correlation became,

$$Nu = 2 + 0.19 \left(\frac{1}{B}\right)^{0.24} Re^{0.5} Pr^{0.33} \tag{29}$$

where B is the transfer number proposed by Spalding (1953).

Drops of aqueous sodium sulfate decahydrate at a concentration of 40 wt. % were dried at air temperatures of 20, 40.7, 59.3, and 78.3°C. The measured temperatures were corrected for radiation and conduction along the thin film thermocouple as described above; the results of the drying rates and core temperatures are listed by Cheong (1983). Figure 5 shows the drying curve and the core temperature history measured simultaneously by the thermocouple at an air temperature of 20°C. There was an initial transient period in the core temperature curve before equilibrium was established and the core temperature reduced to the wet-bulb temperature. The core temperature then rose steadily as the resistance to heat and mass transfer increased with crust thickness. After about 540 s, the measured core temperature rose sharply and reached the air temperature within 70 s. This sudden rise in temperature was caused by the evaporation interface receding beyond the thermojunction, resulting in the dry crust temperature being measured.

The drying curves and core temperature histories at air temperatures of 40.7, 59.3, and 78.3°C are presented in Figures 6, 7, and 8, respectively. The trend of the core temperature curves for these higher air temperatures was somewhat surprising. After the initial transient, the core temperature rose gradually until it reached about 33°C; this was followed by a sudden fall before again increasing steeply to the particular air temperature for the experiment. This phenomenon coincides with the temperature at which sodium sulfate decahydrate crystals melt, about 33°C,

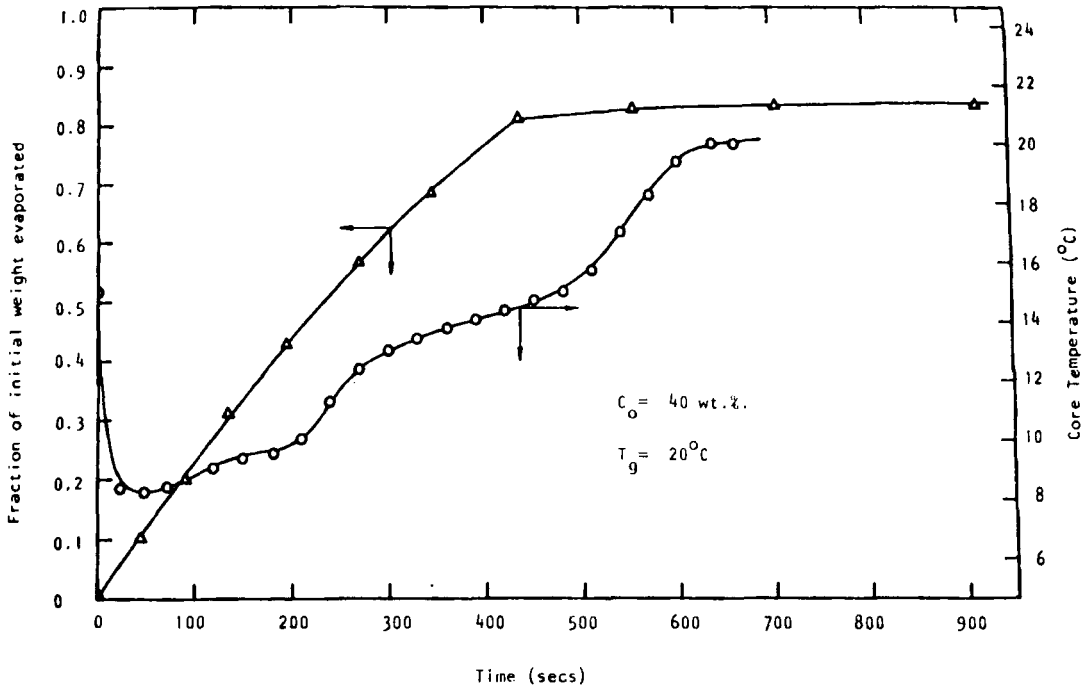

Figure 5. Simultaneous drop weight and core temperature measurements.
T_g = 20°C

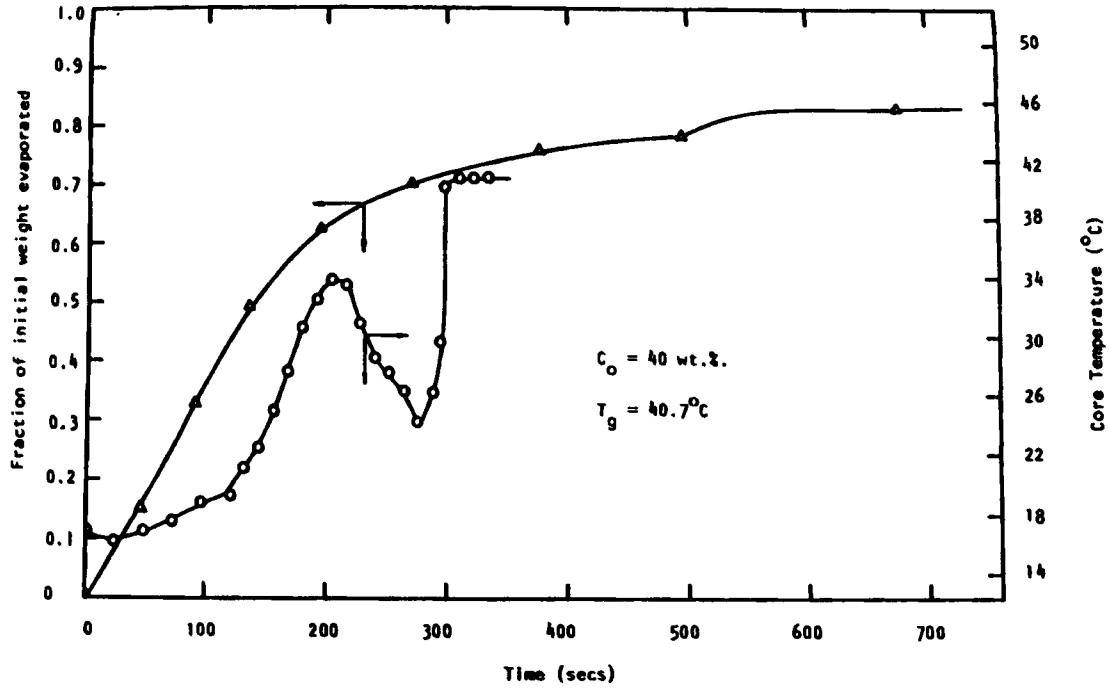

Figure 6. Simultaneous drop weight and core temperature measurements.
T_g = 40.7°C

absorbing heat in the process. This melting and recrystallization occurred very rapidly, resulting in the relatively smooth core temperature curve showing a gradual fall.

The drying curves at all the temperatures investigated show a similar trend to those reported above. As expected, evaporation rates were much higher at higher temperatures, but as soon as a substantial crust was formed the rates reduced significantly.

Comparison of Experimental Results and Model Predictions

The receding interface evaporation model was applied to describe the drying of aqueous sodium sulfate decahydrate with the gas film mass transfer coefficient calculated according to the correlation of Ranz and Marshall (1952) and the gas film heat

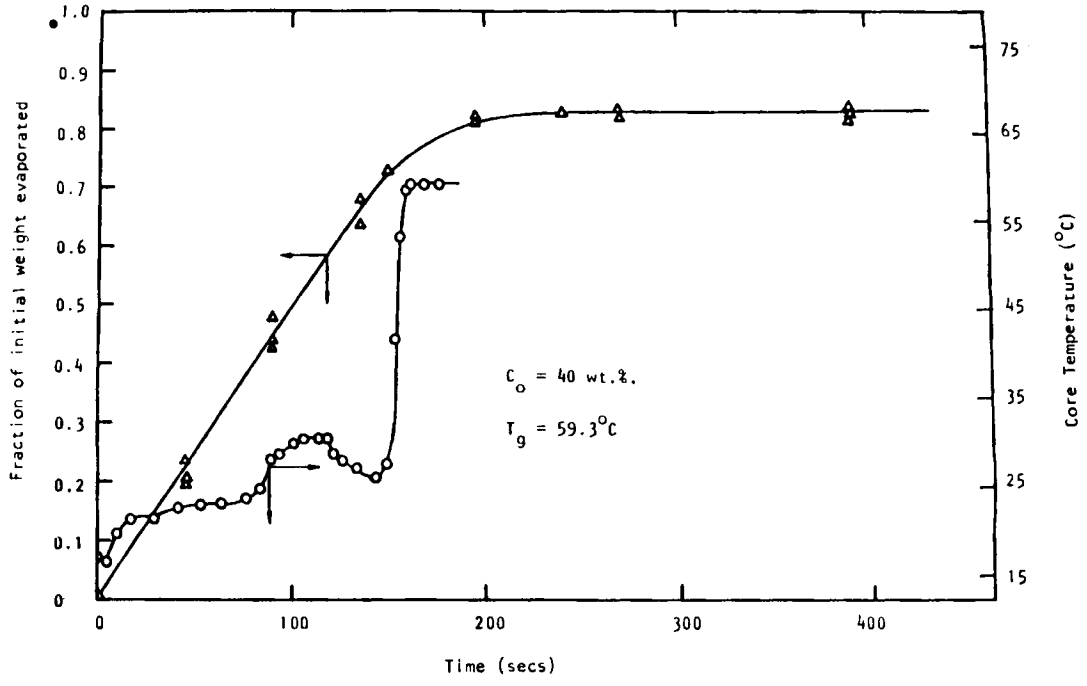

Figure 7. Simultaneous drop weight and core temperature measurements.
T_g = 59.3°C

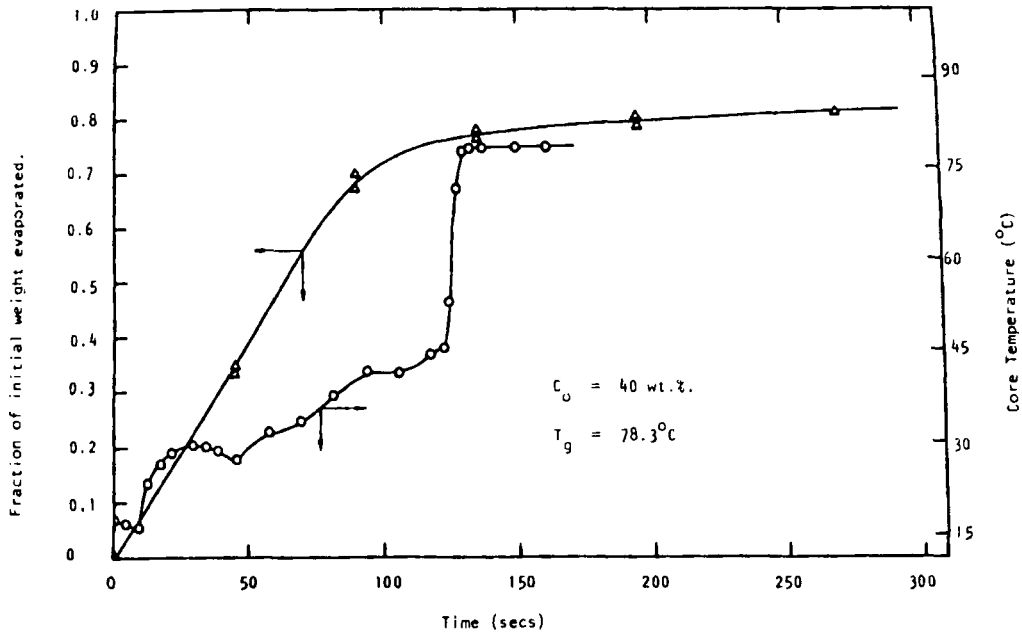

Figure 8. Simultaneous drop weight and core temperature measurements.
T_g = 78.3°C

transfer coefficient calculated from Eq. 28 or 29. The predictions are compared with the results given in Figures 5–8.

The calculation was performed on a microcomputer. A listing of the program, file name REI MODEL, is given by Cheong (1983). The solution of the equations was obtained by a Runge-Kutta fourth-order integration involving simultaneously the variation of core temperature, crust thickness, and drop weight with time. The change of vapor pressure with temperature and the other variables are given in Table 1.

For experiments at air temperatures above 33°C, the model was modified to include an additional heat absorption term to account for the unusual behavior of the decahydrate crystals. Thus

$$\Delta H = \frac{4}{3}\pi R^3 \rho_{co}(1 - x)\lambda_f \tag{30}$$

where λ_f = heat of solution of the decahydrate.
Hence the fall in drop temperature ΔT_s is

$$\Delta T_s = \frac{\Delta H}{WC_{pc}} \tag{31}$$

Equation 31 was included as a subroutine, file name CORE TEMPERATURE, in the above program (Cheong, 1983).

The experimental core temperature history at an air temperature of 20°C is compared to that predicted by the model in Figure 9. The agreement can be seen to be excellent up to about 540 s, when the measured temperature rose sharply, unlike the gradual increase predicted by the model. The reason for this discrepancy has been explained above. That is, the measured temperature after this period was that of the crust while the model continued to predict the actual core temperature. This discrepancy during the final stages of the drying process was also evident at the higher air temperatures.

Figures 10, 11, and 12 present a comparison of the predicted temperatures with the experimental core temperatures at air temperatures of 40.7, 59.3, and 78.3°C, respectively. The modification included to account for the latent heat of fusion at 33°C has correctly predicted a fall in temperature comparable to that of the experimental data. The trend of the curves is in good agreement with the experimental data points, but not as good as that at 20°C.

The predicted crust thickness curves under the same experi-

Table 1. Variables Used in Model

Initial concentration of sodium sulfate decahydrate	40 wt.%
Core density	1,221.8 kg · m^{-3}
Heat capacity of core (Glasstone, 1940)	4,180 J · kg^{-1} · K^{-1}
Heat of crystallization per kg of water evaporated	152 J · kg^{-1}
Latent heat of fusion (Glasstone, 1940)	+239 × 10^3 J · kg^{-1}
Thermal conductivity of crust	0.015 W · m^{-1} · K^{-1}
Partial pressure of drying medium	1.61 × 10^{-4} atm
Variation of vapor pressure with absolute temperature (*Int. Critical Tables*, 1933)	$\log_e p_c = -\frac{5{,}104.05}{T_s'} + 20.21$ where p_c = vapor pressure (mm Hg)
Effective diffusivity (Audu and Jeffreys, 1975)	$D_{eff} = D_v\epsilon^{1.5}$ evaluated at mean crust temperature

SI conversion: kPa = mm Hg × 0.133.

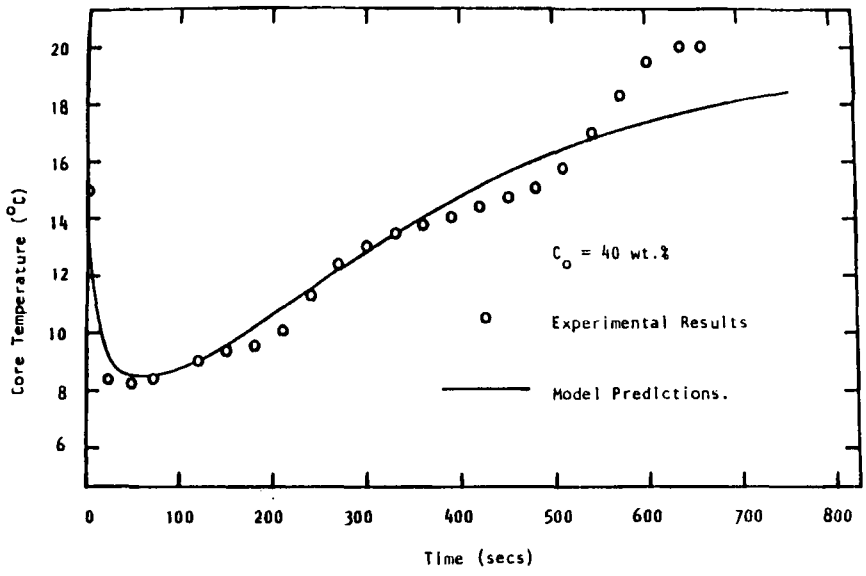

Figure 9. Comparison of experimental core temperatures with model predictions.
T_g = 20°C

mental conditions are presented in Figure 13. Measurements were made only on completely dried particles because it was impossible to obtain measurements from the partially dried particles. When a partially dried particle was removed from the wind tunnel the sudden cooling caused rapid crystallization, which gave an erroneous crust thickness measurement.

The drying curves predicted from the model agree reasonably well during the first drying period. However, the curves overestimated the weight of the drop during the second period after a substantial crust had formed. Very fine fragments of the dried crust, on fracturing, may have fallen away giving a low measurement, but the final (dry) weight in the experiments is consistent with the initial concentration of 40% and therefore a significant loss of crust is unlikely. It is also possible that the assumptions made in the derivation of the model, e.g., linear temperature gradient, may have been extended beyond a limiting crust thickness.

Discussion

The evaporation of pure liquids has been studied extensively partly because, since there is no crust formation, pure liquid systems are less complex. Commercially, the evaporation of pure liquids, e.g. in fuel atomization, crop spraying, humidification, and similar operations, poses fewer problems than the drying of sprays containing solids.

In the latter, after crust formation has occurred evaporation rates are controlled predominantly by the resistance to moisture diffusion in the pores of the crust. However the structure, and in particular the porosity, of the crust has been ignored largely

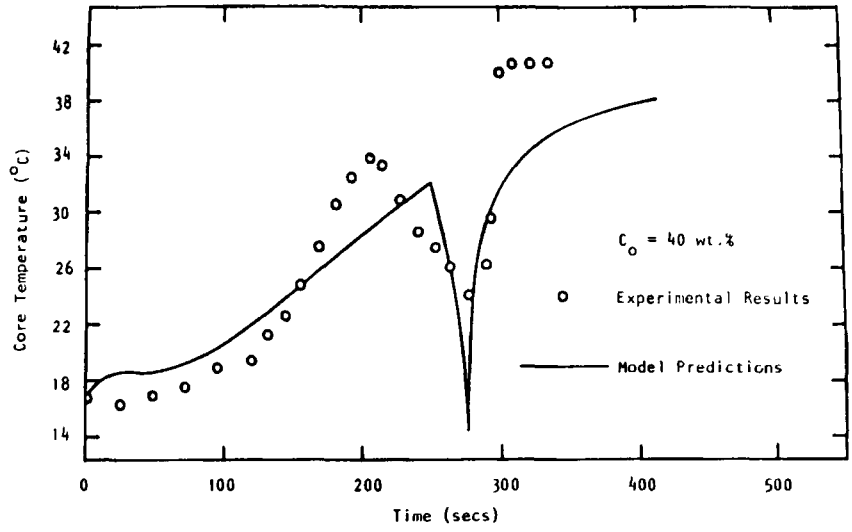

Figure 10. Comparison of experimental core temperatures with model predictions.
T_g = 40.7°C

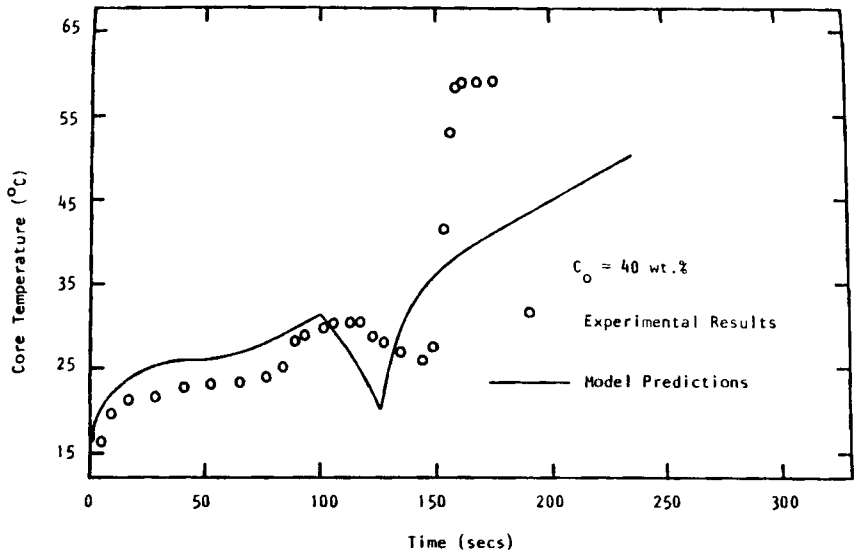

Figure 11. Comparison of experimental core temperatures with model predictions.
T_g = 59.3°C

because of the difficulty in quantifying the parameters. The process becomes even more complex when fractures, shrinkage, or inflation occurs.

The experimental results demonstrated that the behavior of sodium sulfate during drying at temperatures above 33°C is unsual in that it forms different hydrates with incongruent melting points (Glasstone, 1940). Below the transition temperature of 32.4°C, the monoclinic decahydrate crystals are in equilibrium with the liquid phase. At the transition point, the rhombic crystals of anhydrous sulfate commence to separate and exist in equilibrium with the decahydrate and the saturated solution. From the transition point up to about 125°C, the solubility of the anhydrous sulfate actually decreases with increasing temperature. The shape of the core temperature curves shows this behavior clearly at air temperatures above 33°C by the sudden fall at about the transition point. The fall in temperature resulted in a sudden increase in the temperature driving force and consequently the heat and mass transfer rate. This invariably caused rapid evaporation and an increase in the crust growth rate, which resulted in the core temperature rising immediately. As the temperature increased, the crust growth rate was further enhanced by the negative solubility of the anhydrous sulfate. This in turn increased the core temperature even higher. The depression of the core temperature curves at about the transition point appears to be less drastic at the higher air temperature, as is evident from Figures 6 and 8. This was a result of the higher heat transfer rates at the higher air temperatures, tending to very rapidly reestablish the equilibrium.

The enantiomophic change occurs at temperatures between 30 and 35°C over about 60 s, which is sufficient for the complete change, thereby releasing 0.51 kg water per kg of decahydrate. The air velocity over the particle in these experiments was never

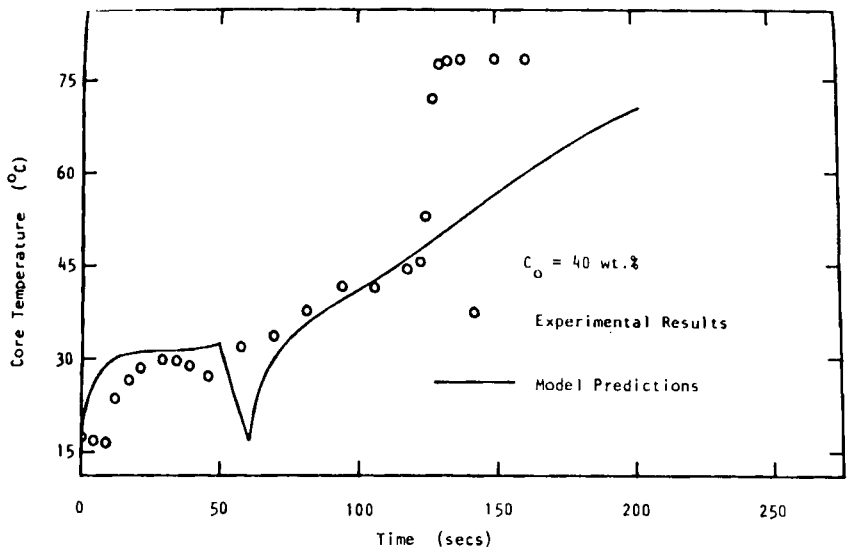

Figure 12. Comparison of experimental core temperatures with model predictions.
T_g = 78.3°C

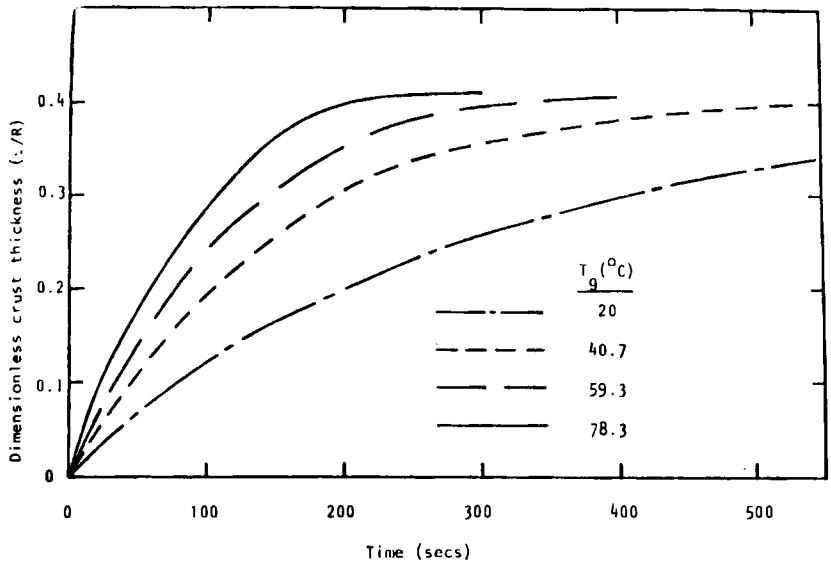

Figure 13. Model predictions of crust thickness as a function of time.
Initial concentration = 40 wt. %

greater than 1 m/s so that the subsequent drop in temperature is unlikely to approach the wet-bulb point in such a short time interval, which would require a velocity of at least 5 m/s and a longer period. Consequently one possible explanation of the phenomenon is as follows. The water is released from within the core of the particle, which hitherto comprises a saturated solution plus solids. The solution is now momentarily unsaturated and is therefore capable of dissolving sodium sulfate to resaturate the liquid in the slurry. In so doing the heat of solution is absorbed by the particle, amounting to +239 kJ/kg. This quantity of heat was inserted into eq. 30 and corrected the model from the sudden drop in temperature to given reasonable agreement with the experimental results.

It should be noted that the unusual behavior of sodium sulfate was not evident from the drying curves alone. This clearly highlighted the advantage of the thin film thermocouple as an investigative tool especially when salts, electrolytes, and the like are present.

The modeling of the drying of sodium sulfate decahydrate slurry drops is complicated by the formation of hydrates and the negative solubility of the anhydrous sulfate. However when heats of solutions and enantiomorphic transformations were inserted into the model, reasonably good agreement was obtained between predicted and experimental results at 20°C.

The model predictions at the higher air temperatures were fairly good although not as accurate as that at 20°C. The modification included to account for the heat of solution at 33°C accurately predicted the fall and rise of the core temperature at the transition point. After the transition point, the model underestimated the core temperature because no modification was included for the negative solubility of the anhydrous sulphate. The model predicted the first period of the drying curve reasonably well but overestimated the second period because of the formation of the anhydrous instead of the decahydrate salt at high temperature, with release of water, whereas in the model the rate in the later stages of drying is inhibited by a relatively thick solid crust. Fractures and blow holes could also have resulted in pieces of the crust falling away. The occurrence of fracture, shrinkage, or inflation is dependent on the particular material being dried, the initial solids concentration, and the drying air temperature. Even under identical conditions and concentration, different equisized drops are known to behave quite differently depending on the exact time at which fracture occurs. This uncertainty would, of course, be impossible to model without a further understanding of the precise mechanisms that control these phenomena.

In spite of the complications with sodium sulfate decahydrate slurries, the model proved to be reasonably accurate and would be expected to perform much better with other slurry materials.

Notation

$a_0 = [R(R - z)h_g]/k_{tc}z$
$a_1 = (R^2h_gK_{tc})/[\rho_{co}x(\lambda - C_c)]$
$a_2 = k_{tc} - Rh_g$
$a_3 = R^2h_g$
$a_4 = (Cpc)/[3x(\lambda - C_c)]$
$b_0 = [R(R - z)k_g]/D_{eff} \cdot z$
$b_1 = (R^2D_{eff}M_wk_g)/(\rho_{co} \times R_c)$
$b_2 = D_{eff} - Rk_g$
$b_3 = R^2k_g$
C_c = heat of crystallization per unit mass of water evaporated, J · kg^{-1}
C_p = heat capacity of air, J · kg^{-1} · K^{-1}
C_d = drag coefficient on particle
C_f = drag coefficient on filament
D_{eff} = effective diffusivity, m^2 · s^{-1}
D_v = molecular diffusivity, m^2 · s^{-1}
F_d = drag force on particle, N
F_f = drag force on filament, N
F_t = total drag force, N
g = gravitational constant, m · s^{-2}
h_g = gas film heat transfer coefficient, W · m^{-2} · K^{-1}
J_r = rate of mass transfer, kg · m^{-2} · s^{-1}
k_c = crust coefficient, m · s^{-1}
k_g = gas film mass transfer coefficient, m · s^{-1}
k_{tc} = thermal conductivity of crust, W · m^{-1} · K^{-1}
M_w = molecular weight with water
p = moisture concentration expressed as partial pressure, atm
p_c = vapor pressure of water at core interface, N · m^{-2}

p_g = vapor pressure of water in air, $N \cdot m^{-2}$
Q_R = heat transfer rate at surface of particle, $W \cdot m^{-2} \cdot s^{-1}$
Q_r = heat transfer rate within crust at radius r, $K \cdot m^{-2} \cdot s^{-1}$
Q_z = heat transfer rate at wet core surface, $K \cdot m^{-2} \cdot s^{-1}$
R = particle radius, m
R_c = universal gas constant, $atm \cdot m^3 \cdot kmol^{-1} \cdot K^{-1}$
r = radius within crust, m
T = temperature, K
T_c = temperature of core, $T_c = T_z$, K
T_s^1 = drop temperature, K
x = mass fraction of water
W = mass of water evaporated, kg
z = plane within particle, m

Greek letters

λ = latent heat of vaporization of water, $J \cdot kg^{-1}$
λ_f = heat of solution, $J \cdot kg^{-1}$
ϵ = porosity of crust
ρ_{co} = density of wet core, $kg \cdot m^{-3}$
θ = time, s

Literature cited

Audu, T. O. K., and G. V. Jeffreys, "The Drying of Drops of Particulate Slurries," *Trans. Inst. Chem. Eng.*, **53,** 165 (1975).

Charlesworth, D. H., and W. R. Marshall, "Evaporation from Drops Containing Dissolved Solids," *AIChE J.*, **6,** 9 (1960).

Cheong, H. W., "The Drying of Small Drops of Particulate Slurries," Ph.D. Thesis, Univ. of Aston, Birmingham, England (1983).

Frössling, N., "The Evaporation of Falling Drops" (English version), *Gerlands Beitr. zur Geophysik,* **52,** 170, (1938).

Glasstone, S., *Text Book of Physical Chemistry,* 1st ed. Macmillan, London (1940).

International Critical Tables, 1st ed., Vol. 3, McGraw-Hill, New York (1933).

Langstroth, G. O., C. H. H. Diehl, and E. J. Winhold, "The Evaporation of Drops in Still Air," *Can. J. Res,* **28A,** 574 (1950).

Miura, K., K. Atarashiya, I. Ouchi, and S. Ohtani, "Experimental Study of Drying Characteristics of Single Drops Containing Solids," *Kagaku Kogaku,* **35,** 643 (1971), and *Heat Transfer, Jap. Res.*, **1,** 11 (1972).

Pasternak, I. S., and W. H. Gauvin, "Turbulent Heat and Mass Transfer from Stationary Particles," *Can. J. Chem. Eng.*, **38,** 35 (1960).

Perry, J. H., and C. H. Chilton, eds., *Chemical Engineers Handbook,* 5th ed., McGraw-Hill, Kogakusha Ltd., Tokyo (1973).

Ranz, W. E., and W. R. Marshall, "Evaporation from Drops," *Chem. Eng. Prog.*, **48,** 141, 173 (1952).

Rowe, P. N., K. T. Claxton, and J. B. Lewis, "Heat and Mass Transfer from a Single Sphere in an Extensive Flowing Fluid," *Trans. Inst. Chem. Eng.*, **43,** T14 (1965).

Spalding, D. B., "The Combustion of Liquid Fuels," *4th Int. Symp. on Combustion,* Williams and Wilkins, Baltimore, 847 (1953).

Trommelen, A. M., and E. J. Crosby, "Evaporation and Drying of Drops in Superheated Vapors," *AIChE J.*, **16,** 857 (1970).

Whytlaw-Gray, R., and H. S. Patterson, *Smoke,* Edward Arnold, London 168 (1932).

Manuscript received May 15, 1985, and revision received Nov. 15, 1985.